Supporting Information

Hinkel et al. 10.1073/pnas.1222469111

SI Text

Regional Sea-Level Rise. Local sea-level rise can significantly vary from the global mean (1, 2) (Figs. S1–S3). In the representative concentration pathway (RCP) 8.5 scenario, the spatial SD in 2100 is between 11 cm (HadGEM2-ES) and 16 cm (MIROC-ESM), or 15% and 19% of the global mean sea-level rise under the medium land-ice scenario (Fig. S3). At a few locations, the deviation can be much larger, from relative sea-level drop in the vicinity of ice masses to more than 50% larger sea-level rise than the global mean in other areas (up to 90%, or 65 cm higher than the global mean, in the HadGEM2-ES model in the open-ocean North Atlantic). The patterns are fairly similar across the scenarios (Fig. S3), despite the large range in projected global mean sea-level rise (Figs. 1 and 2). In relative terms, regional variations are slightly larger in the RCP2.6 (SD of 16–21%).

Generally speaking, there is a predominantly latitudinal pattern of regional sea-level rise, with above-average sea-level rise in the tropics and below-average sea-level rise at high latitudes. This is due to the reduced gravitational pull from high-latitude ice masses as they shrink. Note that we use a uniform fingerprint for the glaciers and ice caps, which tends to overestimate sea-level rise at high latitude (especially along the Scandinavian coast and in Western Canada) and slightly underestimate sea-level rise in the tropics (by a few centimeters).

Ocean circulation changes introduce more local features, such as relatively high sea-level rise along the Northeastern United States coast (3) in three of the four models. Other regions with strong mesoscale eddies also show large changes (leading to above- or below-average rise) under climate forcing, such as in the Antarctic Circumpolar and Aghullas currents, around the North Atlantic subpolar gyre, and the Kuroshio current off Japan. Note these very large changes occur far enough from the coast, and are inherently uncertain due to the coarse resolution of climate models.

Attributing Regional Sea-Level Rise to Coastal Segments. Climate-induced coastal sea-level change was attained by overlaying the grids of the general circulation models (GCMs) with the vectorized coastline segmentation of ref. 4. The sea-level change attributed to a coastline segment was then computed as the average of the ocean grid cells overlapping with the bounding box of the coastline segment. In the case that there were no grid cells overlapping, we took the average of the nearest neighbor ocean grid cells.

Attributing Exposed Areas to Coastal Segments. Areas exposed to flooding were calculated within a geographic information system following ref. 4: first, a uniform zone with a width of 0.3° (around 50 km at the equator) was generated along the world's coastline. The zone was in raster format, with a resolution of 30 arcseconds, thus matching the characteristics of the Global Land One-kilometer Base Elevation (GLOBE) dataset. At the borders of the coastline segments and perpendicular to the coast, subzones were generated. By overlaying the zone information with the GLOBE elevation data, the total area of all pixels belonging to specific elevation increments were calculated for every segment. For segments belonging to river deltas, the width of the zone was extended to 1.8° (around 200 km), as in these regions inundation can reach much further inland. A similar process was undertaken for the Shuttle Radar Topography Mission (SRTM) dataset, with the exception of the resolution of the zone layer, which was set at 3 arcseconds, to match the resolution of the elevation information.

Results over Time. Figs. S4–S6 show the impacts over time in terms of the three impact indicators used in this paper. For each combination of socioeconomic scenario (shared socioeconomic pathway, SSP) and adaptation strategy, we present impacts for RCP2.6 and RCP8.5 in terms of the minimum, maximum, and average impacts across the range of digital elevation models (DEMs), population distribution datasets, GCMs, and land-ice scenarios.

Flood Model Validation. Table S1 and Fig. S7 compare the results of this paper against previous national-level assessments. We ran the Dynamic Interactive Vulnerability Assessment (DIVA) model without considering subsidence/uplift.

A number of national assessments followed the same methodology as ref. 5 and estimated the expected number of people flooded per year under current conditions and an arbitrary 1-m rise in sea level, whereas other national assessments estimated the population living below the 1-in-1,000-y extreme water level (6). This provides an opportunity for validation of global models (7, 8). Table S1 and Fig. S7 build on the earlier analyses and compare results from refs. 6 and 8 with new results of this study combining SRTM and GLOBE with the Global Rural–Urban Mapping Project (GRUMP) population model. In terms of the resident population, SRTM tends to underestimate the population, whereas GLOBE overestimates the population, but both models are reasonable. In terms of expected numbers of people flooded, the SRTM model is a better fit, but again both models are reasonable.

Validating the expected annual flood costs computed here is difficult due to a lack of national studies available. According to ref. 9, there have been eight coastal storms with damages exceeding US$ 10 billion since 2000, and subsequently Hurricane Sandy has produced estimated damages of US$ 66 billion. Total damages in these nine storms were US$ 330 billion, or about US $ 25 billion/y. There were many smaller events, and on the other hand, not all this damage was due to flooding with heavy precipitation and wind also being responsible. Hence, this provides an indicative value to compare with flood damages estimated in this paper to US$ 11–40 billion/y in 2010.

1. Slangen A, Katsman C, Wal R, Vermeersen L, Riva R (2012) Towards regional projections of twenty-first century sea-level change based on IPCC SRES scenarios. *Clim Dyn* 38: 1191–1209.
2. Perrette M, Landerer F, Riva R, Frieler K, Meinshausen M (2013) A scaling approach to project regional sea level rise and its uncertainties. *Earth System Dynamics* 4(1):11–29.
3. Yin J, Schlesinger ME, Stouffer RJ (2009) Model projections of rapid sea-level rise on the northeast coast of the United States. *Nat Geosci* 2:262–266.
4. Vafeidis AT, et al. (2008) A new global coastal database for impact and vulnerability analysis to sea-level rise. *J Coast Res* 24(4):917–924.
5. Hoozemans FMJ, Marchand M, Pennekamp HA (1993) *Sea Level Rise: A Global Vulnerability Assessment. Vulnerability Assessments for Population and Coastal Wetlands and Rice Production on a Global Scale* (Delft Hydraulics and Rijkswaterstaat, Delft, The Netherlands), Revised Ed, p 184.
6. Nicholls RJ (1995) *Synthesis of vulnerability analysis studies*, eds Beukenkamp P et al. (Coastal Zone Management Centre and National Institute for Coastal and Marine Management, The Hague, The Netherlands), Publication 4, pp 181–216.
7. Nicholls RJ, Hoozemans FMJ, Marchand M (1999) Increasing flood risk and wetland losses due to global sea-level rise: Regional and global analysis. *Glob Environ Change* 9(1): 69–87.
8. Nicholls RJ (2004) Coastal flooding and wetland loss in the 21st century: Changes under the SRES climate and socio-economic scenarios. *Glob Environ Change* 14(1):69–86.
9. Kron W (2013) Coasts: The high-risk areas of the world. *Nat Hazards* 66(3):1363–1382.

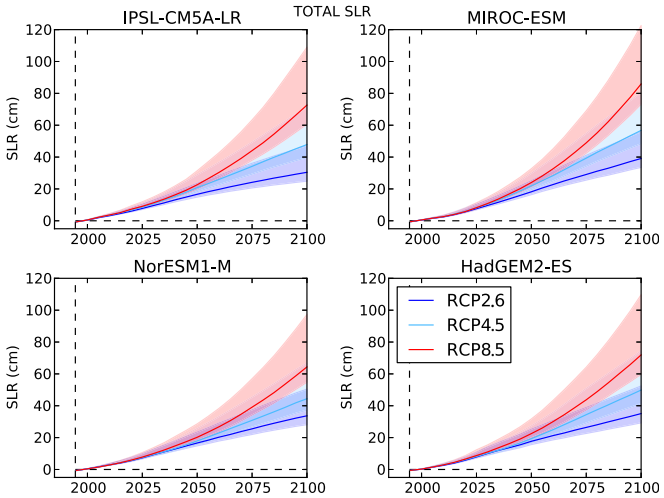

Fig. S1. Global mean sea-level rise relative to 1985–2005.

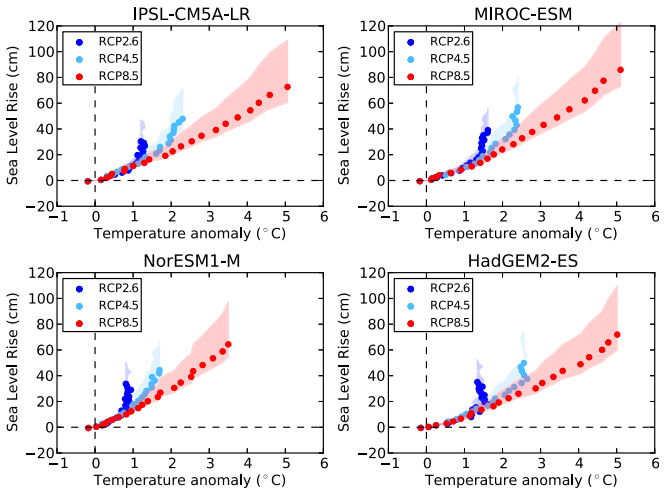

Fig. S2. Global mean sea-level rise relative to 1985–2005 versus global mean temperature anomaly with respect to 1985–2005. The shaded areas show the uncertainty ranges considered here.

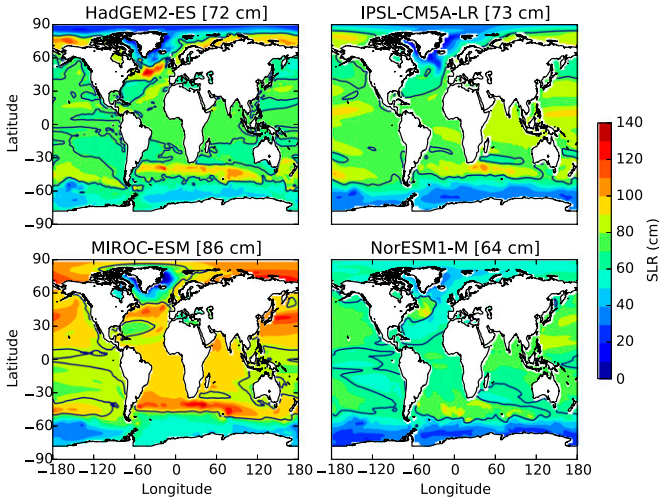

Fig. S3. Median regional sea-level change in 2100 relative to 1985–2005 under RCP8.5 and the medium land-ice scenario.

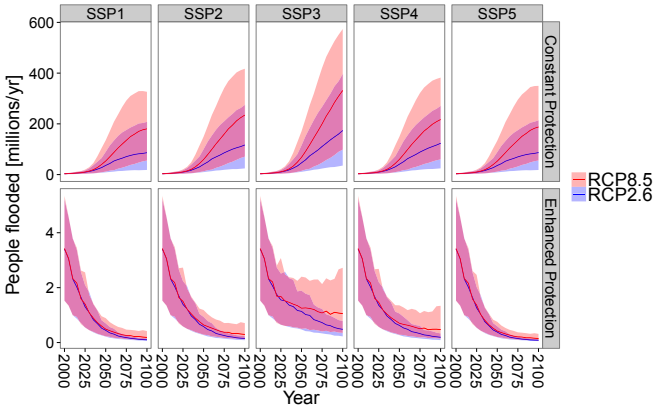

Fig. S4. Global expected annual number of people flooded. The lines show the average impacts across the range of DEMs, population datasets, GCMs, and land-ice scenarios used. The shaded areas show the respective uncertainty ranges defined by the maximum and minimum impacts.

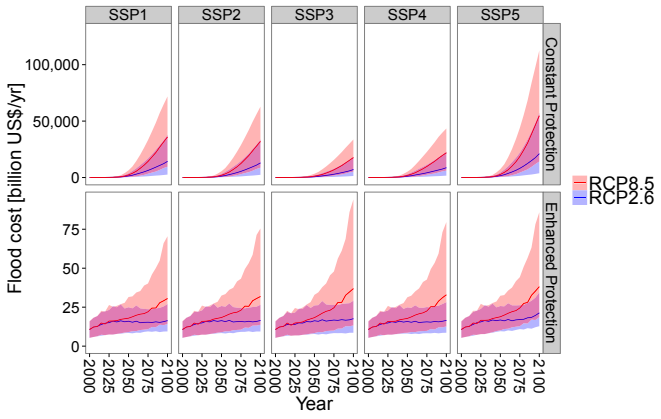

Fig. S5. Global expected annual flood cost. The lines show the average impacts across the range of DEMs, population datasets, GCMs, and land-ice scenarios used. The shaded areas show the respective uncertainty ranges defined by the maximum and minimum impacts.

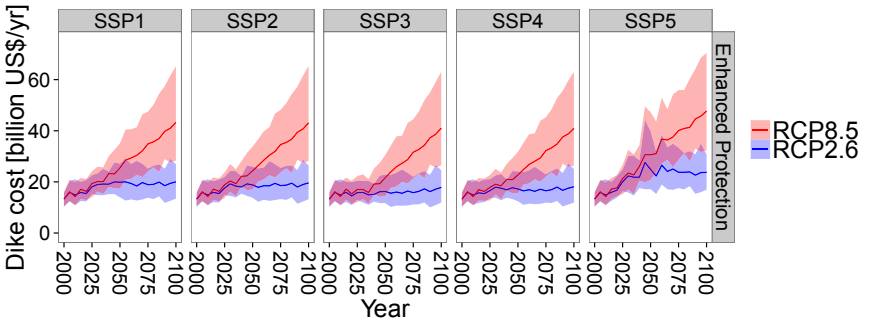

Fig. S6. Global annual dike cost (capital and additional maintenance cost). The lines show the average impacts across the range of DEMs, population datasets, GCMs, and land-ice scenarios used. The shaded areas show the respective uncertainty ranges defined by the maximum and minimum impacts.

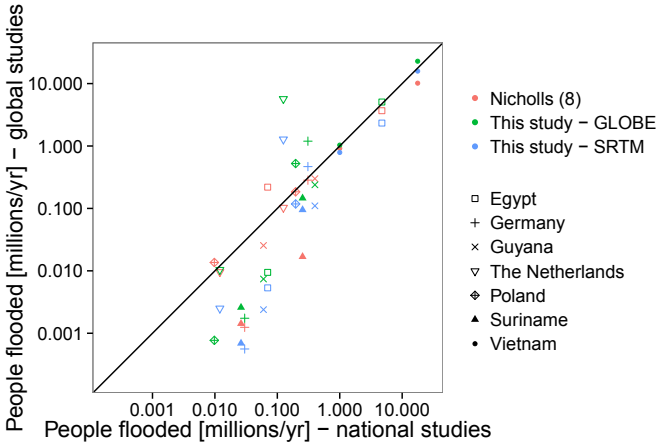

Fig. S7. Comparison of the expected number of people flooded per year estimated by national and global studies for selected countries.

Table S1. Aggregated results from selected national assessments compared with the global model results of ref. 8 and this study

Study	No. of people in millions living below the 1-in-1,000-y extreme water level*	No. of people flooded, millions/y†	
		No sea-level rise	Sea-level rise of 1 m
National studies (6)	154	1.2	23.7
Nicholls (8)	109	1.2	14.7
SRTM (this study)	65	0.8	20.3
GLOBE (this study)	110	1.1	35.7

The socioeconomic scenario being impacted is the 1990 situation in all cases, no adaptation is considered and for population GRUMP is used.
*Antigua, Bangladesh, Belize, Benin, China, Egypt, Germany, Japan, Marshall Islands, Mauritius, The Netherlands, Nigeria, Poland, Suriname, United Kingdom, and Vietnam.
†Egypt, Germany, Guyana, The Netherlands, Poland, Suriname, and Vietnam.